Intermetallic Compounds

DOI: 10.1002/anie.200800378

Structural Complexity in Intermetallic Alloys: Long-Periodic Order beyond 10 nm in the System $BaSn_3/BaBi_3$**

Siméon Ponou, Thomas F. Fässler, and Lorenz Kienle*

Dedicated to Professor Hartmut Bärnighausen on the occasion of his 75th birthday

Structurally complex metallic alloys (CMA) have been the subject of increasing interest in recent years because of their peculiar physical properties, which include order–disorder phenomena, length-scale-related properties, defects, and plastic behavior.[1,2] Long-range-ordered intermetallic alloys are also technically interesting because they exhibit high strength at high temperatures. In these alloys, the yield strength (that is, the stress at which materials begin to deform plastically) increases with increasing temperature. This behavior is abnormal because all other materials usually become softer at higher temperatures.[3] Therefore, understanding the structure–property relationship in this type of alloys is of key interest.

In general, there are several elements to be considered in the structure rationalization of intermetallic compounds. These elements include geometrical factors, such as the atomic sizes,[4,5] the number of valence electrons, the differences in electrochemical potentials, which are related to the electronegativity,[6] and the valence electronic structure of the atoms involved.[7] Intermetallic compounds which consist of at least two metallic components of different electronegativity play a key role in understanding the structure–property relationships and chemical-bonding characteristics in metals. Indeed, in polar intermetallic compounds, the degrees of valence-electron transfer and electron localization vary widely—and almost continuously—with the composition and the nature of the elements involved.[8,9] If the electronegativity difference is high (for example, when electropositive alkali or alkaline earth metals are involved), the valence electrons are transferred to the more electronegative component. In Zintl phases, the atoms of the anionic subunit fulfill the valence rules by forming an appropriate number of bonds ($8-N$ rule).[10] Such a situation is usually observed when mixing s- and p-block metals. As a result, the bonding picture of those systems usually shows coexistence of ionic, covalent, and even metallic interactions.[11]

In contrast, hexagonal and cubic close packings of atoms are good representatives of geometrically controlled structures because they are based on simple principles, such as densest packing of hard, incompressible spheres, symmetry, and coordination.[12] Intermetallic compounds with the composition AE_3, where A is a divalent/trivalent s- or f-block metal and E is a Group 13–15 element, crystallize with distorted close packing of spheres. Ordered variants adopt the $AuCu_3$ ($Pm\bar{3}m$) and Ni_3Sn ($P6_3/mmc$) structure types, with Kagomé nets of E atoms and stacking variants, in analogy to cubic and hexagonal close packings, respectively.[5,12,13] Recently, we reported on such a phase, namely, $BaSn_3$, which exhibits a hexagonal Ni_3Sn-type structure. Structurally, $BaSn_3$ derives from a packing of hard spheres, but electronically it resembles a Zintl phase with localized chemical bonds.[14a] Packing distortion from an ideal hexagonally close-packed array leads to shorter Sn–Sn distances within the layers (relative to the interlayer contacts), which results in triangular Sn_3 units as building blocks. According to the Zintl–Klemm concept, formal electron transfer from Ba to Sn atoms leads to the formula $[Sn_3]^{2-}$, which can be regarded as a polyanionic Zintl anion (with an aromatic π system containing two electrons) that is isoelectronic with the aromatic cyclopropenium unit, $C_3H_3^+$. Interactions between these units through their π systems are strong, and almost equal intra- and inter-ring contacts are observed. The homologous phase $SrSn_3$[15] has *hhcc* stacking and possesses both molecular and metallic structural motifs. Layers with a hexagonal sequence (as in $BaSn_3$) contain, again, molecular-type $[Sn_3]^{2-}$ units and alternate with metallic-type layers exhibiting a cubic closed-packed layer sequence (as in $AuCu_3$). The two phases, $BaSn_3$ and $SrSn_3$, are electrical conductors—and even superconductors at temperatures below 2.4 and 5.4 K, respectively.[14b,15]

Here, we report a systematic study of the effect of partial Bi-versus-Sn substitution on the structure and bonding of the system $BaSn_{3-x}Bi_x$ (with $x = 0.4$–1.0). Various new intermediate structures—including examples with periodic order up to 39 atom layers—were structurally characterized by single-crystal X-ray diffraction.[16] Additionally, high-resolution transmission electron microscopy (HRTEM) investigations revealed further phases with different stacking sequences in the series $(BaSn_3)_m[Ba(Sn_yBi_{1-y})_3]_n$.

Crystals of compounds **2**–**5** (Table 1) were obtained by fusion of stoichiometric amounts of the elements Ba, Sn, and Bi in metal containers and reaction at high temperatures. The samples were characterized by means of single-crystal X-ray

[*] Dr. S. Ponou, Prof. Dr. T. F. Fässler
Department of Chemistry, Technische Universität München
Lichtenbergstraße 4, 85747 Garching/München (Germany)
Fax: (+49) 89-289-13186
E-mail: thomas.faessler@lrz.tum.de
Dr. L. Kienle
Max-Planck-Institut für Festkörperforschung
Heisenbergstrasse 1, 70569 Stuttgart (Germany)

[**] The authors thank V. Duppel for practical TEM work, Prof. A. Simon for enabling the TEM experiments, and Dr. S. D. Hoffmann for susceptibility measurements.

Supporting information for this article is available on the WWW under http://www.angewandte.org or from the author.

 © 2008 Wiley-VCH Verlag GmbH & Co. KGaA, Weinheim

Table 1: Single crystals of polytypes observed in the quasi-binary system $BaSn_3/BaBi_3$.

Refined composition x in $BaSn_{3-x}Bi_x$ (compound number)	Formula parameters $(BaSn_3)_m[Ba(Sn_yBi_{1-y})_3]_n$				Jagodzinski notation	Space group	Cell parameters [Å][a]		
	m	n	n/m	y[b]			$a=b$	c	c/a[c]
0.00 (**1**)	1	0	0	–	h	$P6_3/mmc$	7.253	5.496	1.516
0.43 (**2**)	3	1	0.33	0.43	$(hhhc)_2$	$P6_3/mmc$	7.271(1)	22.165(4)	1.524
0.45 (**3**)	10	3	0.30	0.35, 0.36[d]	$[(hhhc)_2(hhhhc)]_3$	$R\bar{3}m$	7.273(1)	108.04(2)	1.524
0.73 (**4**)	3	2	0.67	0.39	$(hhhcc)_2$	$P6_3/mmc$	7.274(1)	27.943(6)	1.537
0.99 (**5**)	2	2	1	0.33	$(hhcc)_3$	$R\bar{3}m$	7.276(1)	33.713(7)	1.545
3.00 (**6**)	0	1	∞	–	c[e]	$P4/mmm$	5.188	5.157[24]	–

[a] The standard deviations of the last digits are shown in brackets. [b] The value y corresponds to the amount of Sn on the mixed occupied positions in the c-type layers. [c] Ideal ratio for hexagonal close packing (*hcp*): 1.633. The lattice parameters c are scaled to *hcp*. [d] Two mixed occupied positions. [e] Tetragonal distorted.

diffraction, which showed the space groups $P6_3/mmc$ or $R\bar{3}m$.[16] The two phases, $BaSn_{2.57}Bi_{0.43}$ (**2**) and $BaSn_{2.55}Bi_{0.45}$ (**3**), were obtained from the same nominal composition of the starting mixtures but different annealing temperatures, namely, 400 and 500 °C, respectively.[18]

All compounds can be described in terms of stacking of layers composed of either $BaSn_3$ or $Ba(Sn_yBi_{1-y})_3$ (see Table 1). The atoms form distorted hexagonal close-packed layers, and the hexagonal arrangement of Ba atoms in each layer leads to Kagomé nets of Sn and Bi atoms (E). As shown in Figure 1, in the case of compound **2** the layers form along

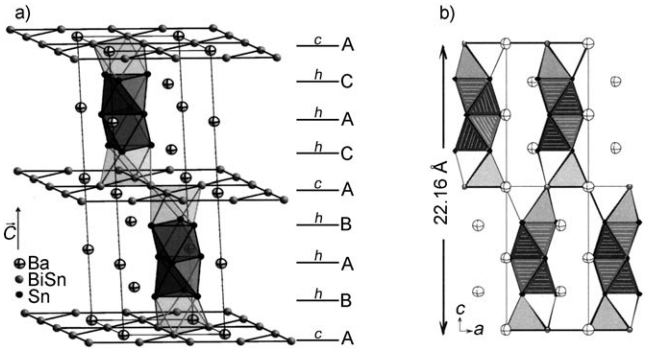

Figure 1. Projection of the structure of $BaSn_{3-x}Bi_x$ (for $x=0.43$). a) Kagomé nets of Sn and Sn/Bi atoms and layer sequences. The resulting face- and vertex-sharing octahedra are shown as dark- and light-grey polyhedra, respectively. b) Parallel projection of (a) showing blocks of face-sharing Sn octahedra (dark color with white hatching) sandwiched between c layers (light-grey polyhedra). The Sn and Sn/Bi sites are drawn as black and grey spheres, respectively, whereas the Ba atoms are represented by crosshatched spheres.

the c-direction hexagonal ($AB\ldots$) or cubic ($ABC\ldots$) packing sequences. Hexagonal (h) and cubic (c) sequences result in face- and vertex-sharing octahedra of E atoms. Compound **2** (with $x=0.43$) crystallizes in the space group $P6_3/mmc$. The unit-cell parameters of **2** are related to those of the parent structure $BaSn_3$, with comparable a parameters ($a=7.256(3)$ Å)[14a] but taking into account a small increase that results from the bigger size of Bi. The c parameter is nearly four times larger than that for $BaSn_3$ (about $4\times5.492(3)$ Å). The translational symmetry along the c axis arises from the stacking of three crystallographically independent close-packed layers alternating with the sequence $ABABACAC\ldots$ or—using the Jagodzinski notation—$(hhhc)_2$. The structure shows an ordered atomic distribution of five of its six crystallographic sites, whereas one site is statistically occupied with Sn and Bi atoms (site 6*g*, 42.2 % Sn occupancy). Notice that all layers with fully occupied Sn positions lead to h stacking, whereas Sn–Bi mixing occurs exclusively in layers with c stacking. For $x=0.45$ (**3**), a rhombohedral symmetry with an intergrowth of a record of 39 layers per unit cell is observed (space group $R\bar{3}m$, No. 166; with $a=b=7.273(1)$ Å, and $c=108.04(2)$ Å). The a and b unit-cell parameters are equivalent to those of **2**, within the standard deviation. Translational symmetry arises from a more complex stacking sequence, namely, $ABABACACACBCBCACACBCBCBA$-$BABCBCBABABACAC\ldots$ (in the Jagodzinski notation: $[(hhhc)_2(hhhhc)]_3$), which results in a very long c axis of 108.05(2) Å. Among the 14 crystallographic positions in **3**, seven are occupied by Ba atoms and five by Sn atoms, and all are ordered; the remaining two positions (sites 9*e* and 18*h*) show Bi/Sn mixing with 35–36 % Sn occupancy. Again, Sn/Bi mixing occurs exclusively in layers with c stacking (see Table 1).

The two structures can be divided in areas of m $BaSn_3$ layers, with an ordered atom distribution, and regions of n $[Ba(Sn_yBi_{1-y})_3]$ layers, with a statistical occupation of Sn and Bi. According to the general formula $(BaSn_3)_m[Ba(Sn_yBi_{1-y})_3]_n$, compound **2** (with $x=0.433$) corresponds to $m=3$, $n=1$, and $y=0.423$. The parameters m and n designate layers with hexagonal and cubic stacking sequences, respectively, whereas the parameter y represents the amount of Sn in positions predominantly occupied by Bi atoms in the c layers.

Similarly, **3** corresponds to $m=10$, $n=3$, and $y=0.35$ and 0.36. Here, the stacking sequence derives from **2** by adding one $BaSn_3$ layer to every third $BaSn_3$ block. As a consequence, the part of the structure with hexagonal layer sequence increases and the n/m ratio decreases. The composition of **3** ($BaSn_{2.55}Bi_{0.45}$) is almost identical to that of **2** ($BaSn_{2.57}Bi_{0.43}$). Note that the formation of an additional layer $BaSn_3$ causes a decrease in the amount of Sn within the c layers (from 42 % for **2** to 35–36 % for **3**) without any noticeable changes in the overall composition. Hence, compounds **2** and **3** reflect an order–disorder transition which is reminiscent of that observed in macroscopic phase segregation.

 © 2008 Wiley-VCH Verlag GmbH & Co. KGaA, Weinheim

At higher Bi contents ($x = 0.73$ and 0.99), two further structures form, namely, **4** and **5**, with a higher number of *c*-type layers, as anticipated by the *n*/*m* ratios of 0.67 and 1.00, respectively. The occupancy factor *y* in the *c* layers remains approximately the same (that is, 0.39 and 0.34 for **4** and **5**, respectively). Increasing the Bi content therefore correlates with the formation of a higher number of mixed Sn–Bi or *c* layers. As a result, long-periodic orders with the sequences $(hhhcc)_2$ and $(hhcc)_3$ and *c* parameters of 27.9 and 33.7 Å are observed for **4** and **5**, respectively.

The *h* layers are fully ordered and contain Ba and Sn atoms at a ratio of 1:3. As in the case of $BaSn_3$, triangular Sn_3 units are predominant; the in-plane shortest contacts, d_{Sn-Sn} and d_{Sn-Ba}, range from 3.00 to 3.04 Å and 3.65 to 3.66 Å, respectively. Antiprismatic stacking of the triangular Sn_3 units along the *c* axis ($d_{Sn-Sn} = 3.27$–3.31 Å) results in elongated face-sharing Sn octahedra which form blocks that are identical (in terms of composition and structure) to a fragment of the $BaSn_3$ structure. In the latter case, $d_{Sn-Sn} = 3.06$ Å is found within the trimers, which are stacked with a Sn–Sn separation of 3.27 Å along the *c* axis. The further in-plane Sn–Sn distance is about 4.2 Å. In **2**, these $BaSn_3$-like blocks are all identical and consist of two face-sharing Sn octahedra separated by a *c* layer (see Figure 2a). Compound **3** contains two different $BaSn_3$-like blocks with two and three condensed Sn octahedra alternating with the ratio 2:1 (see Figure 2c). In all cases, small *c*/*a* ratios (in the range from 1.516 to 1.454) indicate the compression of the cells along the *c* direction, thus suggesting strong interactions between the layers. The *c*/*a* ratio of an ideal hexagonally close-packed structure is 1.633. In the present series, the *c*/*a* ratio increases with higher Bi content (see Table 1).

The much shorter Sn–Sn distances within the trimers in the *h* layer, relative to the in-plane distances between the atoms of two Sn_3 trimers (greater than 4.5 Å) and Sn–Ba contacts (approximately 3.65 Å), hint for directed bonds and covalent contributions to the bonding between the atoms of the Sn_3 units. In contrast, there is no strong distance segregation in the *c*-type layers. The E–E and Ba–E distances are almost equal (about 3.63–3.64 Å). The relatively long interatomic distances in the cubic-type layers account for delocalized (metallic) interactions.

HRTEM and selected-area electron diffraction (SAED) were applied to probe for disordered or periodic structural variations not identified by XRD. All observed samples contain **3** as the relevant product; however, in exceptional cases marginal byproducts were also identified (see below). As a rule, the SAED patterns recorded on **3** exhibit no significant diffuse scattering, thus supporting the ordered stacking of *c* and *h* layers (see Figure 3a, zone axis [100], $d_{003} \approx 36.0$ Å, and the line scans in the Supporting Information). Additionally, tilting experiments around *c** are consistent with the metrics of **3**, and the intensity recorded on thin areas agrees well with kinematical simulations based on the average structure determined by XRD (see the Supporting Information). Only occasionally, the reflections inside the [*uv*0] patterns were elongated along *c**, as expected for a non-periodic sequence of layers. Next to these selected areas, large domains with distinct repeating units of about 22 and 50 Å

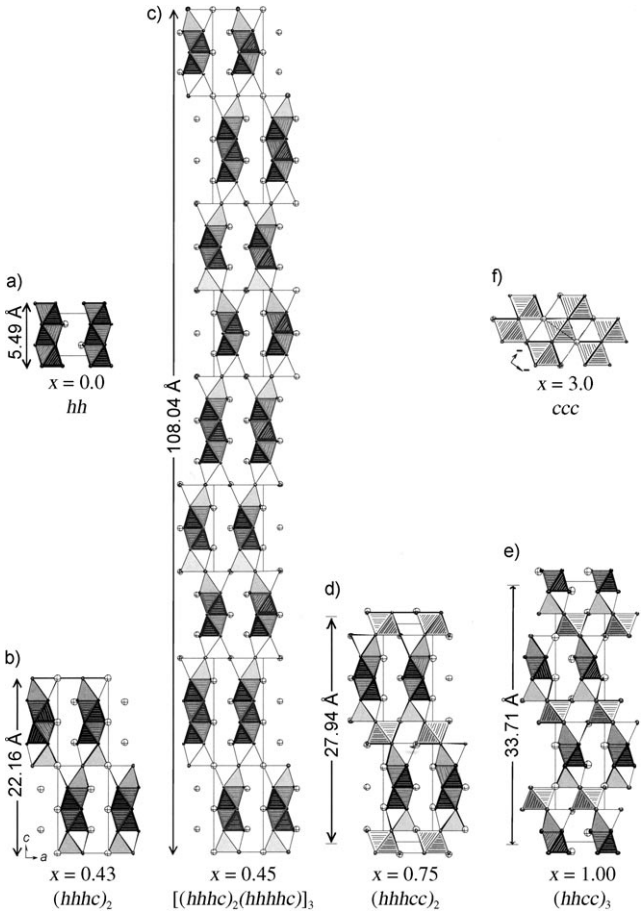

Figure 2. Structure sections of the polytypes in the homologous series $(BaSn_3)_m[Ba(Sn_yBi_{1-y})_3]_n$ (see Table 1) represented as octahedral polyhedra of Sn and E atoms (with E = Sn or Bi). Sn polyedra of hexagonal $BaSn_3$ blocks are shown in dark color with white hatching, whereas E polyhedra of cubic $Ba(Sn_{1-x}Bi_x)_3$ blocks are shown in light grey with black hatching. The unit cells (black lines) are shown on the same scale and the *c* axes are represented in the vertical direction. a) $BaSn_3$ (**1**) ($n = 0$), b) **2** ($m = 3$, $n = 1$), c) **3**, ($m = 10$, $n = 3$) with two different hexagonal blocks containing two and three condensed (face-sharing) Sn octahedra; d) **4**, ($m = 3$, $n = 2$) with a multilayer cubic substructure, e) **5** ($m = 2$, $n = 2$), and f) $BaBi_3$ (**6**).

(see Figure 3b,c) became evident, the first corresponding to **2**. Again, the SAED patterns recorded inside these domains contain only Bragg intensities (see the line scans in the Supporting Information). HRTEM studies confirm that **2** is composed of layered motifs with a thickness corresponding to two *hhhc* stacks.

Since the crystals are extremely sensitive under the conditions applied for HRTEM, only the images recorded immediately after adjusting the zone axes contain essential information. The high-resolution image of Figure 4a (zone axis [100]) displays the *c* and *h* layers edge-on, as demonstrated by the inserted simulated micrograph and the attached polyhedral representation. The bright spots correlate with the cavities of the structure between the rows of atoms. The separation into *c* and *h* layers is evident (see arrows). The *c* layers are imaged as lines of grey spots that sandwich three and four lines of bright spots, which represent the *h* layers.

 © 2008 Wiley-VCH Verlag GmbH & Co. KGaA, Weinheim

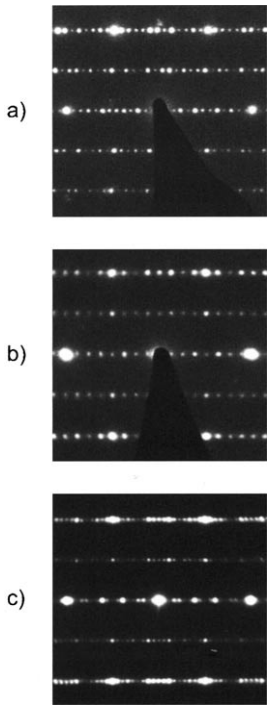

Figure 3. SAED patterns exhibiting distinct repeating units along *c** (referring to the trigonal structure model of **3**). Repeating units of a) approximately 108 Å, b) approximately 22 Å, and c) approximately 50 Å.

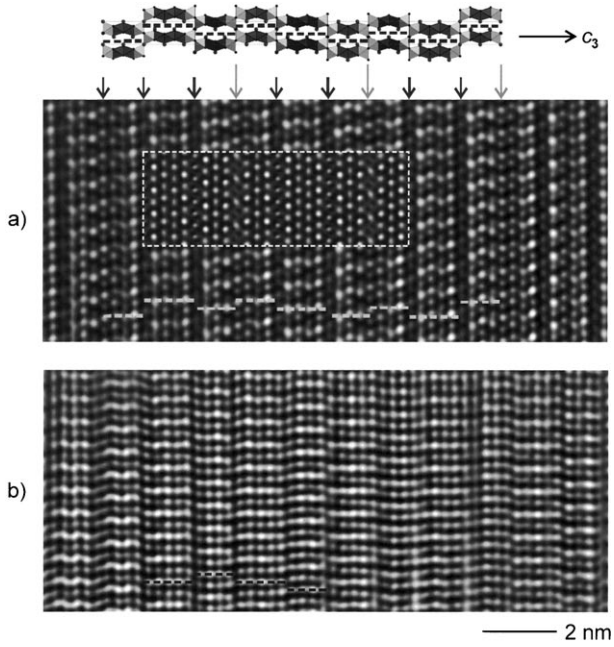

Figure 4. HRTEM studies on **3** (a), zone axis $[100]_{trig}$ with inserted micrograph (occ.$(Bi)_{18h}=1$, occ.$(Sn)_{18h}=0$, occ.$(Bi)_{9e}=0$, occ.$(Sn)_{9e}=1$, $\Delta f=-65$ nm, $t=7.3$ nm). b) Structure variant with a repeating unit of 50 Å.

Hence, *hhhc* and *hhhhc* stacks (with a thickness of about 11 and 14 Å) can be easily identified, their relative positions being consistent with the *R* centering of **3** (see grey dotted lines). The high-resolution micrograph underlines that the complex stacking of the *c* and *h* layers produces a giant repeating unit of approximately 108 Å. On closer inspection, local deviations of the real structure from the average model of the XRD examinations can be identified, particularly concerning the distribution of Bi and Sn atoms inside the *c* layers. Frequently, the *c* layers in the centers of the $(hhhc)_2$ double stacks (see grey arrows in Figure 4a) approximate the neighboring *h* layers. As a consequence, the double stacks appear as one thick stack. This feature can be interpreted by an aggregation of Sn atoms inside the *c* layers. Simulated micrographs convincingly match the experimental images when assuming such an aggregation (see the insert of Figure 4a and the simulations shown in the Supporting Information).

The image in Figure 4b displays a hitherto unknown stacking variant which is composed of two layered motifs exhibiting the thicknesses of the *hhhc* and *hhhhc* stacks (see grey dotted lines in Figure 4b). The repeating unit (of about 50 Å) determined from fast Fourier transforms of the HRTEM images coincides with the value obtained in the SAED experiments (see Figure 3c). Stacking of the motifs and the repeating unit can be rationalized by a sequence of $(hhhhchhhc)_2$.

Compounds **2** to **5** all have intermediate close-packed structures which are recombinations of the simple parent structures, $BaSn_3$ and $Ba(Bi/Sn)_3$, and can be periodically divided into blocks of the $BaSn_3$ type (with strongly anistropic interactions) and slabs of composition $BaBi_3$ (with more isotropic interactions). The formation of $Ba(Bi/Sn)_3$-type blocks of very specific lengths can be interpreted to be the driving force for the long-range ordering in the system Ba/Sn/Bi. In analogy to the binary system, $BaSn_3$, we can assume a formal charge transfer from Ba to Sn in the ternary system, as well as a partial electron localization, according to Ba^{2+}-$[Sn_3]^{2-}$. However, this charge transfer only occurs in *h*-type layers, thus allowing a strong distortion, which is driven by the formation of localized bonds between the Sn atoms in the 2π-electron system $[Sn_3]^{2-}$.[14]

Partial substitution of Sn by Bi leads to the formation of *c*-type-structure blocks of the form: $Ba(Sn/Bi)_3$. In these layers, a solid solution is observed—characterized by a narrow composition range of 34–42 % Sn on the Bi positions and almost equal interatomic distances. The annealing temperature can shift the Sn/Bi ratios in each layer within this composition range, thus inducing changes from the *c*- to the *h*-type structures—or vice versa—as expressed by the *n*/*m* ratio shown in Table 1. In addition to the known structure changes in pseudo-binary Laves phases, where stacking variants up to ten layers have been observed,[20] the pseudo-binary system composed of $BaSn_3/BaBi_3$ shows stacking variants up to 39 layers, an extraordinary ordering on specific atom positions, and giant unit cells as observed for CMAs.

The structural complexity in several intermetallic structures with comparably simple compositions, such as $NaCd_2$, was discussed in a recent review by Lee and Hoffmann,[21] in which structural complexity was rationalized by the partition of the bonding pattern into polar (localized) and nonpolar (metallic) regions; the same concepts may also apply here. The structural complexity in the family of compounds studied

 © 2008 Wiley-VCH Verlag GmbH & Co. KGaA, Weinheim

herein stems from the simultaneous existence of different cluster connectivities and mixed site occupancies with a relatively wide homogeneity range. A formally charge-balanced but metallic Zintl phase $BaSn_3$, which shows some degree of electron localization, intergrowths on the atomic level with regions of isotropic-bond character in the Bi-richer part. The compound $BaSn_3$ was described as a model superconductor in which the superconducting state arises from pairing localization of the conducting electrons.[15] Magnetic susceptibility measurements of **2** and **3** show Pauli paramagnetism, but no bulk superconductivity was found down to 1.8 K.[22]

Here, we demonstrate that the structure of $BaSn_3$ is not stable toward an increase in the valence-electron count, because the system reacts to the addition of electron-richer Bi atoms by creating cubic-type close-packed layers with nonpolar interactions—typical for pure intermetallic phases. Therefore, the structural theme variation that is observed in $BaSn_{3-x}Bi_x$ upon Sn-versus-Bi substitution emphasizes a very peculiar electronic situation of the genuine phase $BaSn_3$, where any increase in the valence-electron count is forbidden. In contrast to this, semiconducting Zintl phases with covalent interactions can be heavily doped without significant structural distortions,[8b] and the typical intermetallic Laves phase KBi_2 shows that partial Bi-versus-Pb substitution leads (over a large range) to a solid solution. However, as soon as the band filling reaches a pseudo-gap, a strong distortion of the structure is observed.[23]

Received: January 24, 2008
Published online: April 17, 2008

Keywords: crystallography · intermetallic phases · solid-state structures · stannide · X-ray diffraction

[1] S. Samson in *Developments in the Structural Chemistry of Alloy Phases* (Ed.: B. C. Giessen), Plenum, New York, **1969**, p. 65.
[2] K. Urban, M. Feuerbacher, *J. Non-Cryst. Solids* **2004**, *334/335*, 143.
[3] M. Feuerbacher, C. Metzmacher, M. Wollgarten, K. Urban, B. Baufeld, M. Bartsch, U. Messerschmidt, *Mater. Sci. Eng. A* **1997**, *233*, 103.
[4] a) P. Villars, L. D. Calvert, *Pearson's Handbook of Crystallographic Data for Intermetallic Phases*, 2nd ed., American Society of Metals, Metals Park, **1991**; b) W. B. Pearson, *The Crystal Chemistry and Physics of Metals and Alloys*, Wiley-Interscience, New York, **1972**.
[5] F. Laves, *Theory of Alloy Phases* (Ed.: E. U. Cleveland), ASM International, Materials Park, **1956**.
[6] a) E. Zintl, *Angew. Chem.* **1939**, *52*, 1; b) W. Klemm, *Angew. Chem.* **1950**, *62*, 133.
[7] W. Hume-Rothery, *J. Inst. Met.* **1926**, *35*, 309.
[8] a) G. J. Miller in *Structure and Bonding of Zintl Phases and Ions* (Ed.: S. Kauzlarich), VCH, New York, **1996**; b) R. Nesper, *Prog. Solid State Chem.* **1990**, *20*, 1.
[9] a) R. Nesper, *Angew. Chem.* **1991**, *103*, 805; *Angew. Chem. Int. Ed. Engl.* **1991**, *30*, 789; b) T. F. Fässler, S. Hoffmann, *Z. Kristallogr.* **1999**, *214*, 722.
[10] E. Zintl, *Angew. Chem.* **1939**, *52*, 1; W. Klemm, *Proc. Chem. Soc. London* **1959**, 329; H. Schäfer, B. Eisenmann, W. Müller, *Angew. Chem.* **1973**, *85*, 742; *Angew. Chem. Int. Ed. Engl.* **1973**, *12*, 694.
[11] T. F. Fässler, *Chem. Soc. Rev.* **2003**, *32*, 80–86.
[12] U. Müller, *Inorganic Structural Chemistry*, Wiley, New York, **1993**.
[13] a) For instance, $BaPb_3$[13b] has *hhc* stacking whereas $SrPb_3$[13c] crystallizes in the $AuCu_3$ type, with *cc* stacking; b) D. E. Sands, D. H. Wood, W. J. Ramsey, *Acta Crystallogr.* **1964**, *17*, 986; c) E. Zintl, S. Neumayr, *J. Less-Common Met.* **1966**, *11*, 308.
[14] a) T. F. Fässler, C. Kronseder, *Angew. Chem.* **1997**, *109*, 2800; *Angew. Chem. Int. Ed. Engl.* **1997**, *36*, 2683; b) T. F. Fässler, S. Hoffmann, C. Kronseder, *Z. Anorg. Allg. Chem.* **2001**, *627*, 2486.
[15] T. F. Fässler, S. Hoffmann, *Z. Anorg. Allg. Chem.* **2000**, *626*, 106–112.
[16] Structure determination**:** All structures were solved from single-crystal diffraction data [$Mo_{K\alpha}$ radiation with a graphite monochromator, 293(2) K], using single crystals selected in an argon-filled glove box and sealed in a glass capillary (with a diameter of 0.3 mm). Data collection was carried out on an Enraf–Nonius CCD diffractometer with rotating anode and a Nonius DIP diffractometer with image plate detector. For crystal data, see Table 1. Structure refinement details in the order: chemical formula, measured reflections, independent reflections, R_1 and wR_2 (all data): (**2**) $Ba_4Sn_{10.27}Bi_{1.73(3)}$, 14134, 510, 0.030, 0.094; (**3**) $Ba_{13}Sn_{33.19}Bi_{5.81(4)}$, 23243, 1281, 0.037, 0.065; (**4**) $Ba_5Sn_{11.34}Bi_{3.66(6)}$, 17061, 508, 0.039, 0.094; (**5**) $Ba_2Sn_{4.03}Bi_{1.97(4)}$, 11116, 401, 0.061, 0.152. An empirical absorption correction was applied using the program SADABS.[17a] The crystal structures were solved by using direct methods (SHELXS-97)[17b] and refined on F^2 by means of full-matrix least-squares methods (SHELXL-97),[17c] with anisotropic displacement parameters for all atoms. Disorder was checked with all atomic positions, but only the Bi positions in the *c* layers were found to be partially substituted by Sn atoms. Further details on the crystal-structure investigation(s) may be obtained from the Fachinformationszentrum Karlsruhe, 76344 Eggenstein-Leopoldshafen, Germany [fax: (+49) 7247-808-666, e-mail: crysdata@fiz-karlsruhe.de] on quoting the depository numbers CSD-419206 (**1**), CSD-419044 (**2**), CSD-419029 (**3**), CSD-419031 (**4**), and CSD-419030 (**5**).
[17] a) H. D. Flack, *Acta Crystallogr. Sect. B* **1983**, *44*, 505; b) G. M. Sheldrick, *Acta Crystallogr. Sect. A* **1990**, *46*, 467; c) G. M. Sheldrick, *SHELXL-97*, *Program for the Solution and Refinement of Crystal structures*, University of Göttingen, Germany, **1997**.
[18] Mixtures (about 1.0 g) of elemental barium (rod, 99.3%), tin (tears-shape, 99.999%), and bismuth (granules, 99.999%) with the nominal compositions (see Table 1) were loaded into a niobium ampoule under inert-gas (argon) atmosphere. After sealing the ampoule, the sample was heated (at a rate of 150 K h^{-1}) to 1073 K for three hours and then cooled at −150 K h^{-1}. Samples **2** and **3** were annealed (at 673 and 773 K, respectively) for ten days and subsequently cooled (at 60 K h^{-1}) to room temperature. All the products obtained were air- or moisture-sensitive, crystalline, and exhibited a silvery color with metallic luster.
[19] a) The samples were crushed under dry argon and transferred to the microscope inside an argon-filled bag. Qualitative energy dispersive X-ray (EDX) analysis confirms the absence of contaminants. Electron microscopy examinations were performed using a Philips CM30 ST (300 kV, Cs = 1.15 mm, LaB_6 cathode, Gatan multiscan CCD camera). The beam sensitivity of the samples forced the use of low-dose settings. The multislice formalism[19b] was used for image simulations; b) P. A. Stadelmann, *Ultramicroscopy* **1987**, *21*, 131.
[20] Y. Komura, *Acta Crystallogr.* **1962**, *15*, 770; F. Laves, H. Witte, *Metallwirtsch. Metallwiss. Metalltech.* **1935**, *14*, 645.
[21] D. C. Fredrickson, S. Lee, R. Hoffmann, *Angew. Chem.* **2007**, *119*, 2004; *Angew. Chem. Int. Ed.* **2007**, *46*, 1958.

 © 2008 Wiley-VCH Verlag GmbH & Co. KGaA, Weinheim

[22] Magnetic susceptibility data were collected for samples of compounds **2** and **3** between 1.8 and 300 K on a Quantum Design MPMS 5S instrument. The samples were cooled in the absence of a magnetic field, previously checked by an external Hall probe. After the introduction of a magnetic field, the data were recorded while the sample was warmed ("shielding") and then cooled ("Meissner"). Superconducting transitions at 3.7 and 4.4 K for samples of **3** annealed at 573 and 673 K suggest the presence of very small amounts of Sn and $BaSn_5$ impurities, respectively. No other kinks were observed in the cooling curves of the samples, which suggests the absence of further superconducting phases down to 1.8 K.

[23] S. Ponou, N. Müller, T. F. Fässler, U. Häussermann, *Inorg. Chem.* **2005**, *44*, 7423.

[24] N. N. Zhuravlev, V. P. Melik-Adamyan, *J. Phys. Chem. Solids* **1970**, *31*, 2653 – 2662.

 © 2008 Wiley-VCH Verlag GmbH & Co. KGaA, Weinheim